www.czasopisma.pan.pl PAN POLSKA AKADEMIA NAUK www.journals.pan.pl

Arch. Metall. Mater. **68** (2023), 2, 447-453

DOI: https://doi.org/10.24425/amm.2023.142421

JINLING YU[1], ZHENG ZHENTAI[1*], SHUAI LI[1], DONGHUI GUO[1], LIANG CHANG[1]

# EFFECTS OF $Y_2O_3$ ON MICROSTRUCTURE AND CORROSION PROPERTIES OF LASER CLADDING COMPOSITE COATINGS ON 304 STAINLESS STEEL SUBSTRATE

Ni625/WC composite coatings added with different amounts of $Y_2O_3$ were prepared on the surface of 304 stainless steels by laser cladding. This study focused on the microstructure characteristics, microhardness, and corrosion performances of Ni625/WC composite coatings. The results showed that $Y_2O_3$ can effectively improve the corrosion resistance of the composite coatings. The microstructure from the bottom to the surface of composite coatings consists of plane crystal, cellular crystal, columnar crystal and equiaxed crystal. The $Y_2O_3$ content of optimum composite coating was 1.0%. Its microhardness was three times that of matrix material. In addition, the corrosion current density of the composite coating was only 2% of Ni625/WC coating, which was attributed to the good properties of $Y_2O_3$ and appropriate $Y_2O_3$ refined microstructure.

*Keywords:* Laser cladding; Ni-based coatings; Electrochemical corrosion

## 1. Introduction

304 stainless steels have been widely concerned in pump and valve industry for its good corrosion resistance and mechanical properties [1]. However, some key parts of pump and valve products, such as valve core and shaft, have poor wear resistance under the long-term wear conditions, lose their function due to leakage eventually and result serious economic losses [2]. At the same time, in a highly corrosive environment, 304 stainless steel is difficult to meet actual working conditions [3]. In order to improve the service life of the work piece and save costs, certain methods are used to modify the surface of the material to enhance corrosion resistance of the material.

Laser cladding is a kind of material surface modification technology, which can satisfy the quality requirements of key parts of pumps and valves [4,5]. Cermet composite coatings are a research hotspot in the field of laser cladding technology. In recent years, WC has been widely used in laser cladding due to its high hardness, good thermal stability and good wettability to molten metal. There are many reports about metal matrix composite coatings by laser cladding, especially composite coatings are reported which with Ni-based alloy powder and hard particles such as WC. Similarly, coatings with good corrosion resistance have been widely reported [6,7]. Li et al. [8] manufactured Ni-based ceramic composite coatings on medium carbon steel substrate by laser cladding, which had high hardness and good corrosion resistance. Damian Kocle et al. [9] manufactured IN686 coatings with the laser cladding process formed an effective barrier against corrosion of the 13CrMo4-5 steel.

Rare earth (RE) elements have strong surface activity, and generate high melting point, low density, relatively stable rare earth compounds with molten metal that contains low melting point elements. They can be used as the core of heterogeneous nucleation to improve the nucleation rate and make the grains smaller. RE elements play the role of solution strengthening, microstructure refinement and structure purification in composite coatings [10].

## 2. Experimental Materials and Methods

### 2.1. Experimental Materials

The sample materials were 304 stainless steels with dimensions of 50 mm × 80 mm × 10 mm. Their original hardness were 230 HV. The powders morphology analyzed by an optical microscope (OM) were shown in Fig. 1. The chemical compositions of 304 stainless steels were presented in TABLE 1.The cladding material consisted of Ni625 with sizes ranging from 20 μm to 53 μm (TABLE 2), WC with sizes ranging from 50 μm to 100 μm and $Y_2O_3$ powders with sizes ranging from 20 nm to 60 nm.

[1] HEBEI UNIVERSITY OF TECHNOLOGY, SCHOOL OF MATERIALS SCIENCE AND ENGINEERING, NO. 5340, XIPINGDAO ROAD, BEICHEN DISTRICT, TIANJIN, 300401, PR CHINA.

* Corresponding author: zzt@hebut.edu.cn

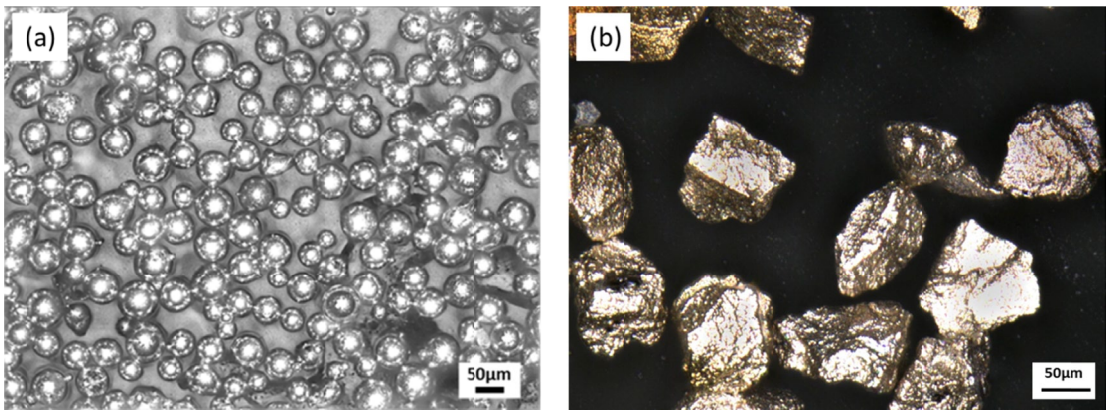


Fig. 1. Morphology of the experimental powders: (a) Ni625, (b) WC

TABLE 1

Chemical composition of the 304 stainless steel (wt. %)

| C | Si | Mn | P | Ni | Cr | S | Fe |
|---|---|---|---|---|---|---|---|
| 0.07 | 0.4 | 1.31 | 0.03 | 7.8 | 16.8 | 0.029 | Bal |

TABLE 2

Chemical composition of the Ni625 alloy (wt. %)

| C | Cr | Si | Fe | Ni | Nb | Mo |
|---|---|---|---|---|---|---|
| 0.08 | 21.19 | 1.09 | 1.85 | Bal | 3.51 | 9.18 |

### 2.2. Experimental Methods

The 304 stainless steels substrates were brushed with a stainless steel wire brush and washed with acetone. Then, mixture powders of Ni625 and WC with a weight ratio of 7:3 was prepared, and one of 0%, 0.5%, 1.0%, 1.5% (wt.) of $Y_2O_3$ powders was added to these mixture. The prepared four mixed powders were completely homogenized using a GN-2 ball mill for 2 h. And the powders were evenly spread on substrates through a preset powder process, and the thickness was approxi-mately 1.0 mm and dried in a vacuum furnace at 150°C for 2 h. The multi-track-joined laser cladding process were conducted using a 1.5 kW TDJG-1 Multi Axis CNC laser processing Machine. The optimum processing parameters were as follows: laser power, 1 000 W; spot diameter, 2.0 mm; scanning speed, 6.0 mm/s; and overlapping rate, 40%. Argon was used as protective gas, and the flow rate was 10 L/min to prevent the composite coatings from oxidation. In addition, the substrates were preheated to 300°C before cladding to reduce the occurrence of cracks.

Samples were cut into sizes of 10 mm × 10 mm × 10 mm by a molybdenum wire cutting machine. After grinding and polishing, a 10% oxalic acid was used to corrode the samples for 10 s. The qualities and morphologies of the composite coatings were analyzed by using a Leica DM2700 optical microscope (OM) and a HITACHI S-4800 SEM (Hitachi, Tokyo, Japan) equipped with an energy dispersive spectroscope (EDS). The phase compositions of composite coatings were analyzed by a Smartlab 9 kW X-ray diffractometer (Rigaku, Akishima, Japan) with the Cu-Kα radiation at 40 kV and 100 mA. Microhardness of composite coatings from the surface to the substrate were measured by a Shimadzu HMV-2T Vickers hardness tester under a load of 0.98 N and a dwell time of 10 s. Corrosion resistance of four kinds of composite coatings were tested by Princeton versastat 3F electrochemical workstation. The corrosion solution was 3.5% NaCl solution prepared by deionized water. A three-electrode system was applied in the present study, in which a platinum foil, a saturated calomel electrode (SCE) and the specimen were used as auxiliary electrode, reference electrode and working electrode, respectively. Effective working area of the specimens was 1 $cm^2$. All the samples were immersed in the electrolyte solution for 1 h to stabilize the open-circuit potential. Scanning range of the potentiodynamic polarization curve was –0.5 to 0.2 V, and the scanning rate was 0.001 $mV \cdot s^{-1}$. An alternating current (AC) electrochemical impedance spectroscopy (EIS) test was performed at the open-circuit potential with voltage amplitude of 10 mV and a frequency range of $1\times10^{-2}$ Hz to $1\times10^{5}$ Hz.

## 3. Results and Discussion

### 3.1. Phase Analysis of the Coatings

XRD of the composite coatings with different $Y_2O_3$ content are shown in Fig. 2. Obviously, the addition of RE don't change phase components. There are slight differences between $Y_2O_3$-free coating and $Y_2O_3$-modified coatings. The results shows that the composite coatings containing $Y_2O_3$ have a new wave crest at about 42°, which is caused by the larger radius of $Y^+$, the larger lattice parameters and the larger crystal plane spacing when the composite coatings are added. The content of $Y_2O_3$ is too low to be detected by XRD. The composite coatings are mainly phase composed of γ(Fe-Cr-Ni), $Fe_3W_3C$ and some carbides such as $Cr_{23}C_6$, $(Fe,Cr)_7C_3$, WC and $W_2C$. Some of the WC particles are transformed into $W_2C$ during laser processing. The XRD pattern shows that a complex chemical reaction occurs between the WC particles and Ni625 during the cladding process, resulting in the generation of a series of complex compounds.

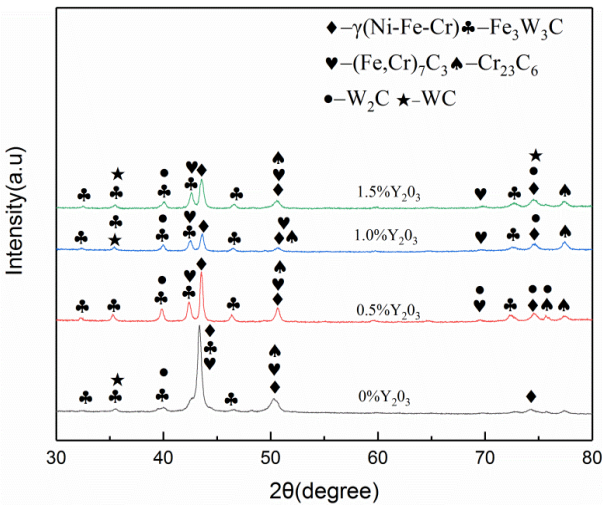


Fig. 2. XRD patterns of different composite coatings

### 3.2. Microstructural Analysis of the Coatings

Fig. 3 shows cross-section of composite coatings with different content of $Y_2O_3$. The surface of composite coatings is smooth and continuous without any pores, cracks, or other defects, and the metallurgical bonding between coatings and substrate are excellent. The microstructures of four coatings are composed of dendrite and eutectic structure. Obviously, the grain sizes of composite coatings modified by RE oxides are refined compared to those without RE oxides. The reason may be that $Y_2O_3$ has purify effect for composite coatings, it shows strong chemical activity in process of solidification, and reacts with impurities in composite coatings, thereby reducing the solid solubility of impurities in composite coatings [11]. Besides this, grain sizes of the coating with a content of 1.0% are significantly better than the content of other two $Y_2O_3$. This indicates that

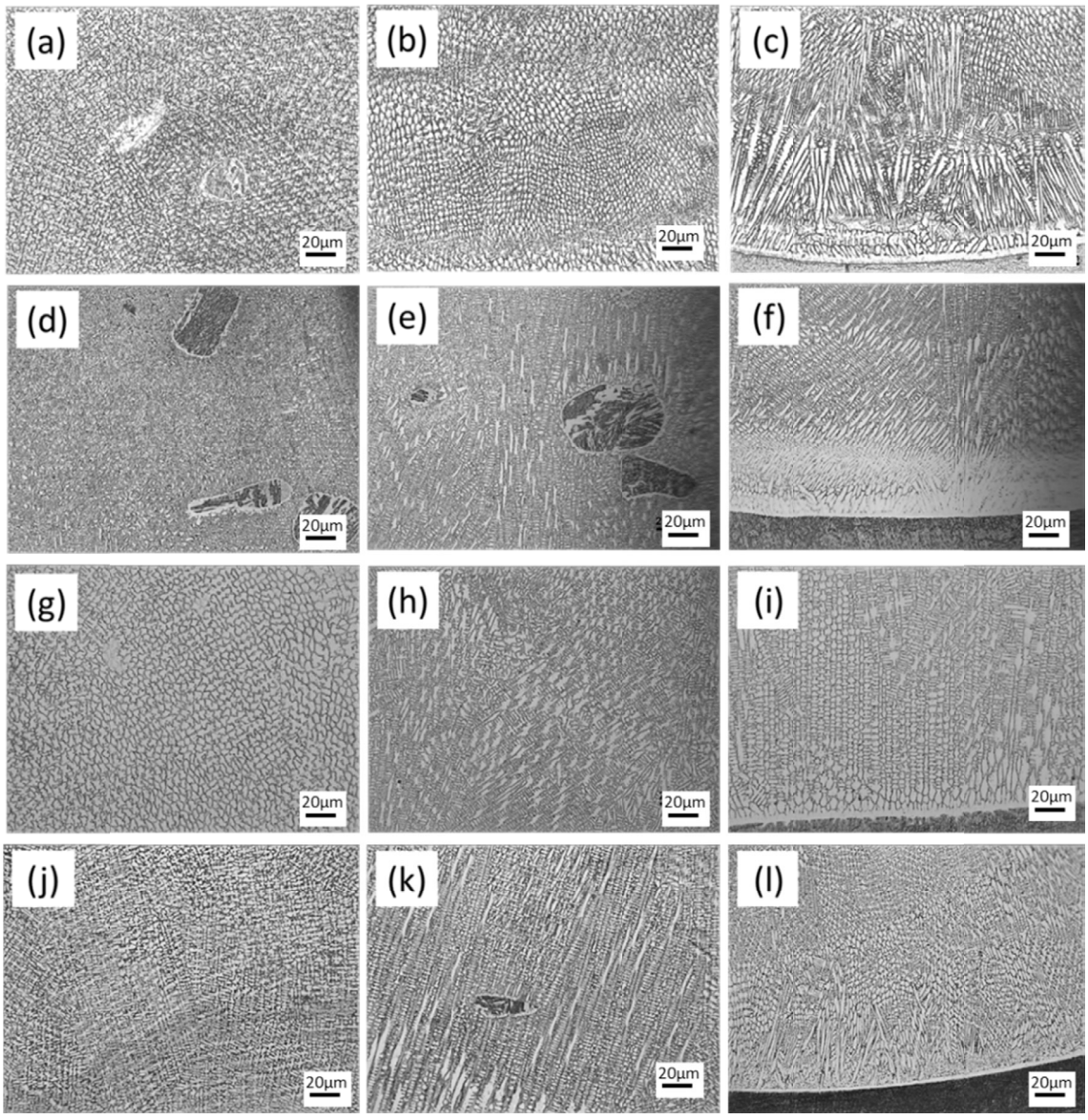


Fig. 3. Microstructure of $Y_2O_3$-modified composite coatings: (a) the top, (b) middle, and (c) bottom part of the composite coating when no rare earth is added; (d) the top, (e) middle, and (f) bottom part of the composite coating modified using 0.5% $Y_2O_3$; (g) the top, (h) middle, and (i) bottom part of the composite coating modified using 1.0% $Y_2O_3$; (j) the top, (k) middle, and (l) bottom part of the composite coating modified using 1.5% $Y_2O_3$

presence of excessive $Y_2O_3$ has played a role in reducing fluidity of molten pool, which causes deceleration of convection speed, increases the difficulty associated with discharge of inclusions, as a result, the final grain sizes become larger.

As cooling rate of composite coatings during melting increased from the top to the bottom, their microstructure changed significantly, from equiaxed crystal to dendrite crystal, cellular crystal to planar crystal. Compared to the sample without modification of RE elements, grain sizes of samples with a modification of RE elements are greatly refined.

After laser cladding is applied, microstructure of coatings are dependent on supercooling of components, the temperature gradient (G) and the solidification rate (R) in the liquid at the solid-liquid interface frontier [12]. The ratio of the temperature gradient to the solidification rate, G/R, is the largest at the interface of composite coating and the 304 stainless steel, decreasing successively toward the surface of composite coating. The greater the G/R is, the larger the supercooling rate is, which indicated that supercooling rate at the interface of composite coating and 304 stainless steel substrate is the largest, leading to the formation of a plane crystal at the interface. When the supercooling rate continued to decrease, precipitates with dendrite structure are formed and grew. As the composite coating/air interface approaches, the supercooling rate of melt continues to decrease, and new nuclei are formed and grew as equiaxed crystals. Although the addition of RE oxides doesn't change grain composition and arrangement, it changes the grain sizes greatly. Because of small solubility of RE elements in composite coatings, it is hard for XRD to detect them.

In the process of rapid laser heating, solubility of WC in molten pool is bigger than Ni-based alloy powders because WC powders have higher absorption of laser energy. Therefore, some tiny WC particles are completely dissolved, and edge and convex of larger WC particles also appear partly dissolved. Sharp corner position of WC particles have a higher surface free energy that makes RE segregate on their surface, as shown in Fig. 4.

### 3.3. Microhardness Analysis of the Coatings

Fig. 5 shows microhardness results of composite coatings. It can be clearly seen that hardness of coatings are significantly higher than that of the substrate. It is reported that transition of hardness originates from the formation of inter dendritic carbides and the eutectic structures. Compared with the $Y_2O_3$-free coating, the hardness of coatings with RE additions are greatly improved. The presence of RE decreases nucleation radius of liquid metals and refines grain sizes. At the same time, dissolution and smoothing of WC particles are beneficial to elimination of internal residual stress, especially for the composite coating with 1.0% $Y_2O_3$. Thus, fine grain strengthening and dispersive strengthening enhance hardness of $Y_2O_3$-modified coatings [13].

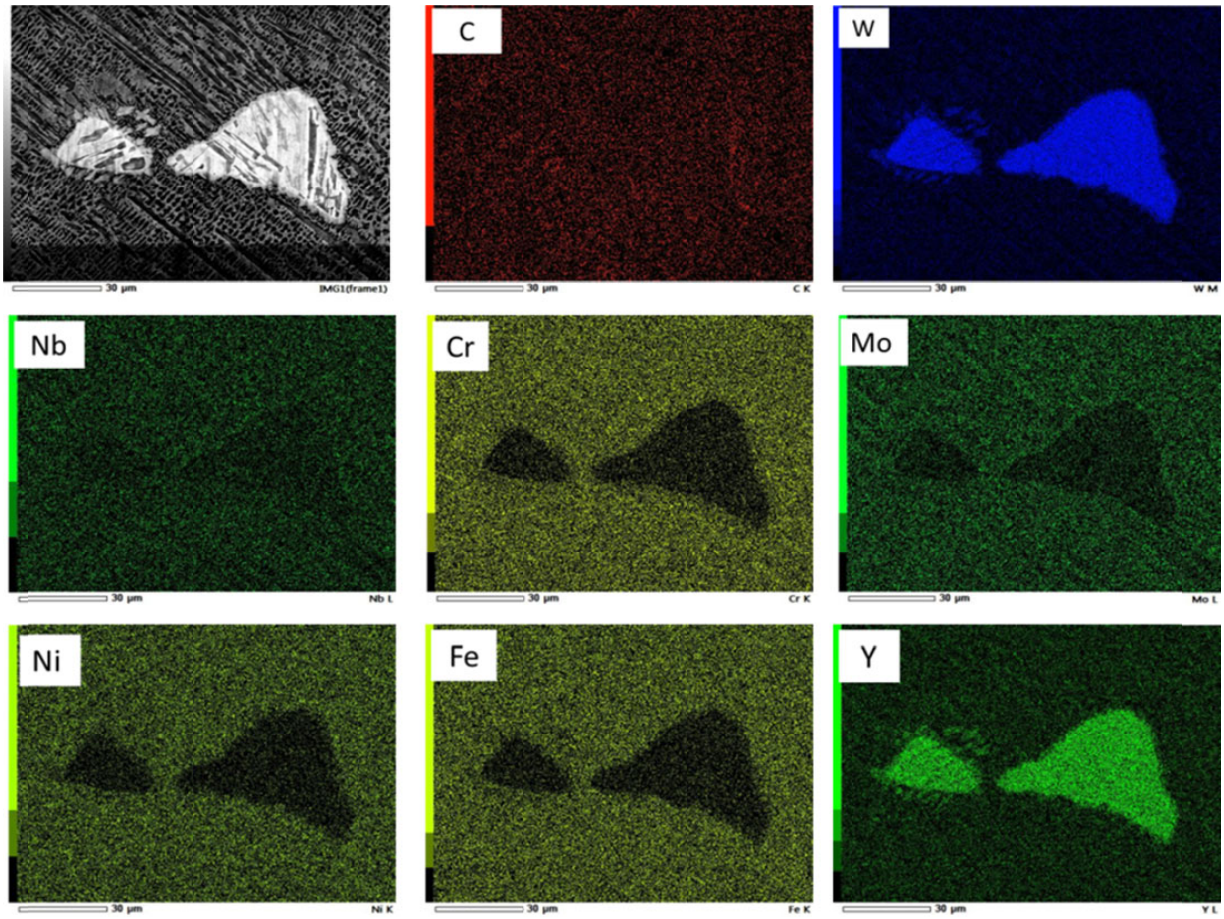


Fig. 4. Distribution of elements in the microstructure of 1.0% $Y_2O_3$ composite coating

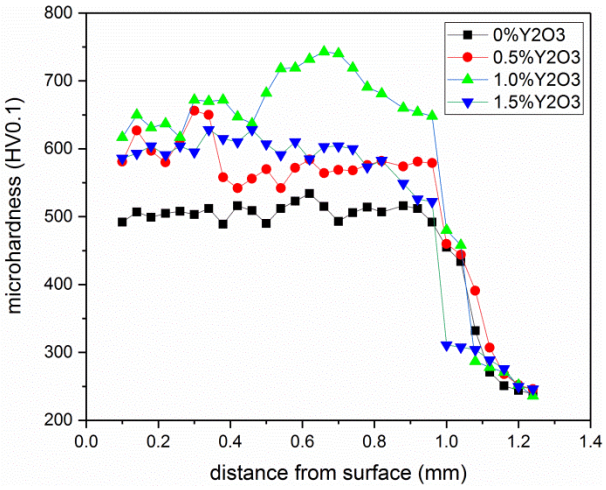


Fig. 5. Microhardness variation in the cross section of composite coatings

corrosion potential ($E_{corr}$) and corrosion current density ($I_{corr}$) are obtained from the intersection point of anodic ($\beta_a$) and cathodic ($\beta_c$) branch of Tafel slopes. Polarization resistance ($R_p$) is calculated using Eq. (1) [14].

$$R_p = \frac{\beta_a * \beta_c}{I_{corr} * 2.303(\beta_a + \beta_c)} \quad (1)$$

The electrochemical corrosion parameters such as $E_{corr}$, $I_{corr}$, $\beta_a$, $\beta_c$, and $R_p$ are tabulated in TABLE 3.

As it is evident from the TABLE 3, the lowest corrosion current density of the $Y_2O_3$-modified composites coatings (0.043 μA/cm$^2$) is 2% that of the $Y_2O_3$-free Ni-based coating (2.198 μA/cm$^2$). However, the highest polarization resistance of the $Y_2O_3$-modified coatings (612.442 kΩ) is about 40.7 times than that of the $Y_2O_3$-free Ni-based alloy coating (15.048 kΩ),

### 3.4. Electrochemical properties

#### 3.4.1. Linear polarization resistance (LPR) measurements

Fig. 6(a) shows the Tafel plots of composites coatings with 0%, 0.5%, 1.0% and 1.5% $Y_2O_3$ in 3.5 wt.% NaCl solution. The

TABLE 3

Corrosion parameters obtained for samples from LPR test

| Sample | $E_{corr}$ (mV) | $I_{corr}$ (μA·cm$^{-2}$) | $\beta_a$ (mV) | $\beta_c$ (mV) | $R_p$ (kΩ) |
|---|---|---|---|---|---|
| 0% $Y_2O_3$ | –189 | 2.198 | 114.6 | 205.3 | 15.048 |
| 0.5% $Y_2O_3$ | –176 | 0.451 | 90.1 | 150.6 | 54.305 |
| 1.0% $Y_2O_3$ | –173 | 0.043 | 169.8 | 93.1 | 612.442 |
| 1.5% $Y_2O_3$ | –181 | 0.048 | 222 | 139.7 | 574.524 |

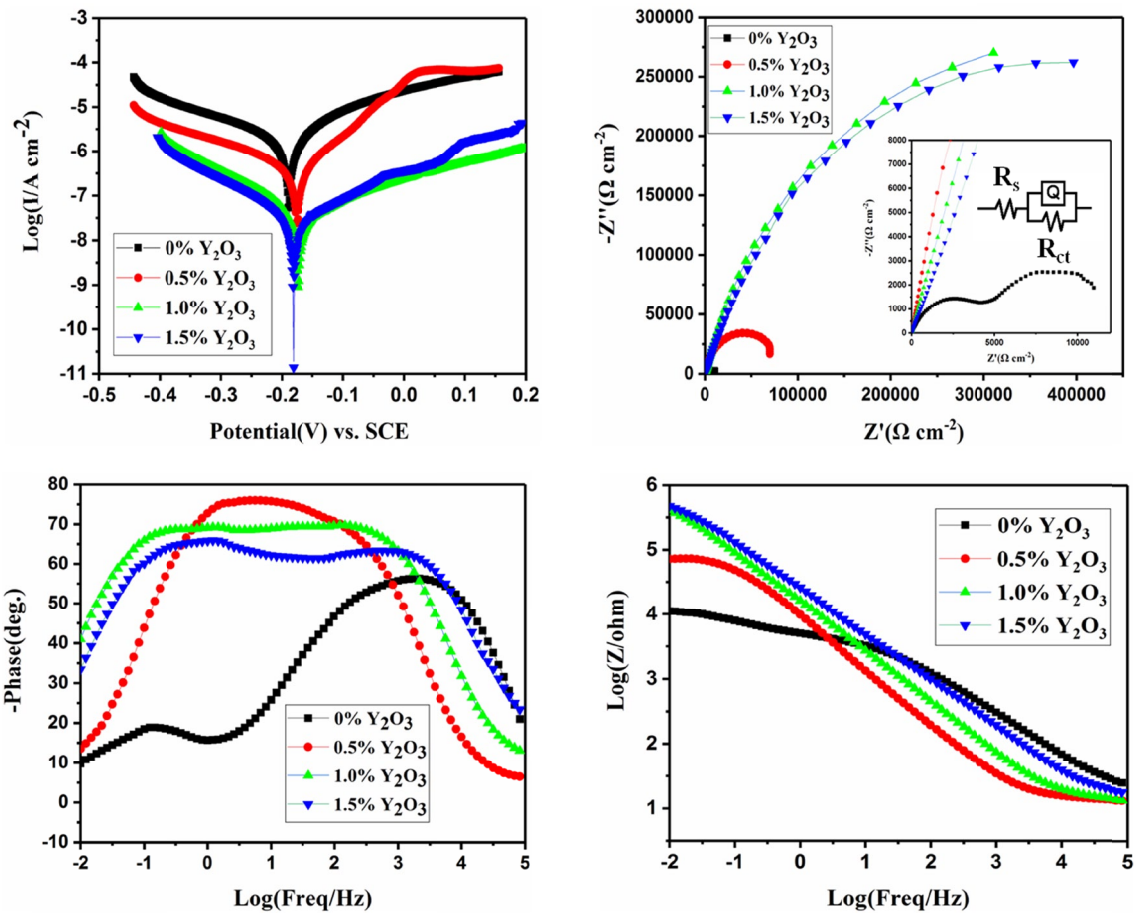


Fig. 6. (a) Tafel plot of composites coatings; (b) Nyquist impedance plot (with insets of enlarged Nyquist plot and equivalent circuit used for fitting); (c) and (d) Bode impedance plot of composites coatings

indicating that $Y_2O_3$ can improve corrosion resistance of Ni-based coatings. It is obvious that the Ni-based composite coating with 1.0 wt.% $Y_2O_3$ has the smallest $I_{corr}$ and the largest $E_{corr}$, the decrease in corrosion current density is an indication of reduction in the corrosion rate, it shows better corrosion resistance when $I_{corr}$ is lower and $E_{corr}$ is higher.

### 3.4.2. Electrochemical Impedance Spectroscopy (EIS)

Nyquist plots of the $Y_2O_3$-free and $Y_2O_3$-modified composite coatings are shown in the Fig. 6(b). Nyquist plots of all samples shows incomplete semicircles arcs. It can be seen that radii of the capacitive impedance loops of $Y_2O_3$-modified coatings are greater than that of $Y_2O_3$-free Ni-based coating. As well known, the larger radius of capacitive impedance loop is, the better is corrosion resistance [15]. Thus, $Y_2O_3$ with 1.0% content can largely improve corrosion resistance of composite coatings. Generally, the ability of inhibiting penetration of electrolyte in composite coatings is related to the middle frequency loop [16]. The larger the middle frequency loop is, the better the corrosion resistance is. In conclusion, the EIS results further confirm that $Y_2O_3$ can enhance corrosion resistance of Ni-based coatings. The EIS spectra of samples are fitted to an equivalent circuit Eq. (2).

$$Z(\omega) = R_s + \frac{1}{\frac{1}{R_{ct}} + i\omega C} \tag{2}$$

The fitted equivalent circuit for 1.0% $Y_2O_3$ Ni-based coating is shown in the inset of Fig. 6(b). Impedance ($Z$) of the coating governs electrochemical reactions at the working electrode and electrolyte interface. Where, $\omega$ is the angular frequency (rad/s) equal to $2\pi f$ and $f$ is the frequency (Hz). $R_s$ represents the solution resistance, $R_{ct}$ is the charge transfer resistance and $C$ is the capacitance (F). The electric double-layer at the interface between the electrode and the solution is generally equivalent to a capacitor, which is called electric double-layer capacitor (EDLC). Because of the "dispersion effect", the frequency response characteristics of EDLC of the solid electrode are not consistent with the "pure capacitance", $Q$ is used to describe the physical quantity when the parameter of capacitance $C$ deviates, which is called constant phase angle element (CPE). The solution resistance $R_s$ is due to the metal ions formed at the interface by electrochemical reactions. The significance of $R_{ct}$ signals indicates interfacial charge transfer, which is the controlling step of the corrosion reaction. The corrosion rate is controlled by the electrochemical reactions and the migration of ions [17].

Owing to complex alloying elements in $Y_2O_3$-modified Ni-based coatings, many metal dissolution reactions can contribute to corrosion rates in anodic branch. Therefore, at the anode, M is defined as metal element in composite coatings. The electrochemical corrosion reactions of M in 3.5 wt.% NaCl solution at room temperature can be written as ($M \rightarrow M^+ + e^-$) and at the cathodic reaction ($2H_2O + O_2 + 4e^- \rightarrow 4OH^-$) as the electrolyte solution is neutral.

Fig. 6(c) and (d) show Bode impedance and Bode phase angle plot respectively, for all coatings tested. The obtained Bode plots have similar shapes for the $Y_2O_3$-modified composites coatings tested. They are symmetrical and have one maximum located in the low frequency range. The highest value of impedance modulus is obtained for 1.0% $Y_2O_3$ coating. This means that a layer of corrosion products forming on the specimen effectively protects the coating against further degradation. This also shows that the results of the Bode plots are consistent with those of the Nyquist plots.

## 4. Conclusions

Ni625/WC composite coatings added with different amounts of $Y_2O_3$ (0%, 0.5%, 1.0% and 1.5%) were prepared on the surface of 304 stainless steels by laser cladding. Effects of $Y_2O_3$ addition on microstructure, phase composition, and corrosion properties were studied, and the following conclusions are obtained.

(1) The addition of $Y_2O_3$ improved the microstructure of composite coatings, the coarse equiaxed crystals and dendrites existed in the $Y_2O_3$-free coating were refined, grain sizes became smaller and spacing between dendrites became narrower. The phase compositions of four Ni-based coatings were composed of γ(Ni-Cr-Fe), $Fe_3W_3C$ solid solution, and hard phases of WC, $W_2C$, $(Fe,Cr)_7C_3$ and $Cr_{23}C_6$.

(2) The modification of RE oxides on composite coatings had further increase hardness and corrosion resistance. In this article, the composite coating with 1.0% $Y_2O_3$ had the best corrosion resistance.

**Acknowledgement**

This work is financially supported by the Natural Science Foundation of Hebei Province, P. R. China under Grant No. E2020202011.

## REFERENCES

[1] X.H. Wang, A.M. Liu, Microstructure and abrasive-wear behavior under high temperature of laser Clad Ni-based WC ceramic coating, Phys. Procedia. **50**, 145-149 (2013). DOI: https://doi.org/10.1016/j.phpro.2013.11.024

[2] Z. Liu, G. Li, J. Li, M. Wang, H. Yu, C. Chen, Wear Properties and Characterization of Laser-Deposited Ni-Base Composites on 304 Stainless Steel, Surf. Rev. Lett. **27**, 1-6 (2020). DOI: https://doi.org/10.1142/S0218625X19502196

[3] R. Aisthi, G. Abraham, S. Kumar, K. Bhattacharyya, N. Keskar, R.P. Kushwaha, R. Rao, R. Tewari, D. Srivastava, G.K. Dey, Corrosion Characteristics of Ni-Based Hardfacing Alloy Deposited on Stainless Steel Substrate by Laser Cladding, Metall. Mater. Trans. A Phys. Metall. Mater. Sci. **48**, 2915-2926 (2017). DOI: https://doi.org/10.1007/s11661-017-4074-1

[4] D. Bartkowski, A. Bartkowska, A. Piasecki, P. Jurči, Influence of laser cladding parameters on microstructure, microhardness, chemical composition, wear and corrosion resistance of Fe-B composite coatings reinforced with B4C and Si particles, Coatings. **10**, 1-18 (2020). DOI: https://doi.org/10.3390/COATINGS10090809

[5] Y.P. Ding, R. Liu, L. Wang, J.H. Li, J.H. Yao, Corrosion and Wear Performance of Stellite Alloy Hardfacing Prepared via Laser Cladding, Prot. Met. Phys. Chem. S. **56**, 392-404 (2020). DOI: https://doi.org/10.1134/S2070205120020069

[6] D. Bartkowski, G. Kinal, Microstructure and wear resistance of Stellite-6/WC MMC coatings produced by laser cladding using Yb:YAG disk laser, Int. J. Refract. Met. Hard Mater. **58**, 157-164 (2016). DOI: https://doi.org/10.1016/j.ijrmhm.2016.04.017

[7] G. Muvvala, D.P. Karmakar, A.K. Nath, Monitoring and assessment of tungsten carbide wettability in laser cladded metal matrix composite coating using an IR pyrometer, J. Alloys Compd. **714**, 514-521 (2017). DOI: https://doi.org/10.1016/j.jallcom.2017.04.254

[8] M. Li, B. Han, Y. Wang, K.J. Pu, Effects of $La_2O_3$ on the microstructure and property of laser cladding Ni-based ceramic coating, Optik. **130**, 1032-1037 (2017). DOI: https://doi.org/10.1016/j.ijleo.2016.11.111

[9] D. Koclęga, A. Radziszewska, S. Dymek, J.H. Li, J.H. Yao, Improvement of Corrosion Resistance of 13CrMo4-5 Steel by Ni-Based Laser Cladding Coatings, J. Mater. Eng. Perform. **29**, 3702-3713 (2020). DOI: https://doi.org/10.1007/s11665-020-04867-x

[10] Y. Hou, H. Chen, Q. Cheng, L. Fan, L. Dong, Effects of Y2O3 on the microstructure and wear resistance of WC/Ni composite coatings fabricated by plasma transferred arc, Mater. Express **10**, 634-639 (2020). DOI: https://doi.org/10.1166/mex.2020.1686

[11] P. Xu, X. Tang, S. Yao, J. He, G. Xu, Effect of Y2O3 addition on microstructure of Ni-based alloy + Y2O3/substrate laser clad, J. Mater. Process. Technol. **208**, 549-555 (2008). DOI: https://doi.org/10.1016/j.jmatprotec.2008.01.026

[12] Z. Xu, Z. Wang, J. Chen, Y. Qiao, J. Zhang, Y. Huang, Effect of rare earth oxides on microstructure and corrosion behavior of laser-cladding coating on 316L stainless steel, Coatings **9**, 1-11 (2019). DOI: https://doi.org/10.3390/coatings9100636

[13] X. He, R.G. Song, D.J. Kong, Microstructures and properties of Ni/TiC/La 2 O 3 reinforced Al based composite coatings by laser cladding, Opt. Laser Technol. **117**, 18-27 (2019). DOI: https://doi.org/10.1016/j.optlastec.2019.04.002

[14] S. Singh, M. Sribalaji, Nitin P. Wasekar, S. Joshi, G. Sundararajan, R. Singh, A.K. Keshri, Microstructural, phase evolution and corrosion properties of silicon carbide reinforced pulse electrodeposited nickel-tungsten composite coatings, Appl. Surf. Sci. **364**, 264-272 (2016). DOI: https://doi.org/10.1016/j.apsusc.2015.12.179

[15] J.Z. Lu, B. Han, C.Y. Cui, C.J. Li, K.Y. Luo, Electrochemical and pitting corrosion resistance of AISI 4145 steel subjected to massive laser shock peening treatment with different coverage layers, Opt. Laser Technol. **88**, 250-262 (2017). DOI: https://doi.org/10.1016/j.optlastec.2016.09.025

[16] N.W. Dai, L.C. Zhang, J.X. Zhang, X. Zhan, Q.Z. Ni, Y. Chen, M.L. Wu, C. Yang, Distinction in corrosion resistance of selective laser melted Ti-6Al-4V alloy on different planes, Corros. Sci. **111**, 703-710 (2016). DOI: https://doi.org/10.1016/j.corsci.2016.06.009

[17] G. Meng, Y. Li, Y.W. Shao, T. Zhang, Y.Q. Wang, F.H. Wang, X.Q. Cheng, C.F. Dong, X.G. Li, Effect of Microstructures on Corrosion Behavior of Nickel Coatings: (II) Competitive Effect of Grain Size and Twins Density on Corrosion Behavior, J. Mater. Sci. Technol. **32**, 465-469 (2016). DOI: https://doi.org/10.1016/j.jmst.2015.11.013